Global Biogeochemical Cycles

Supporting Information for

Reconstructing the pre-industrial coastal carbon cycle through a global ocean circulation model: Was the global continental shelf already both autotrophic and a CO2 sink?

Fabrice Lacroix[1,2,3,] Tatiana Ilyina[1], Goulven G. Laruelle[2] and Pierre Regnier[2]

[1] Ocean in the Earth System, Max Planck Institute for Meteorology, Hamburg, Germany

[2] Department Geoscience, Environment & Society (DGES), Université Libre de Bruxelles, Brussels, Belgium

[3] Max Planck Institute for Biogeochemistry, Jena, Germany

Contents of this file

Introduction

In this supporting information file, further details on the segmentation of continental shelves are given (Text S1), along with information about the derivation of pre-industrial riverine loads (Text S2). In Text S3 descriptions and results of sensitivity experiments for shelf sediment organic matter and terrestrial dissolved organic matter (tDOM) degradation are given. Finally, we provide additional validation basis for oceanic variables (S4-S7).

Text S1. Continental shelf delineations

Continental shelves delineations are given here as used in the main manuscript.

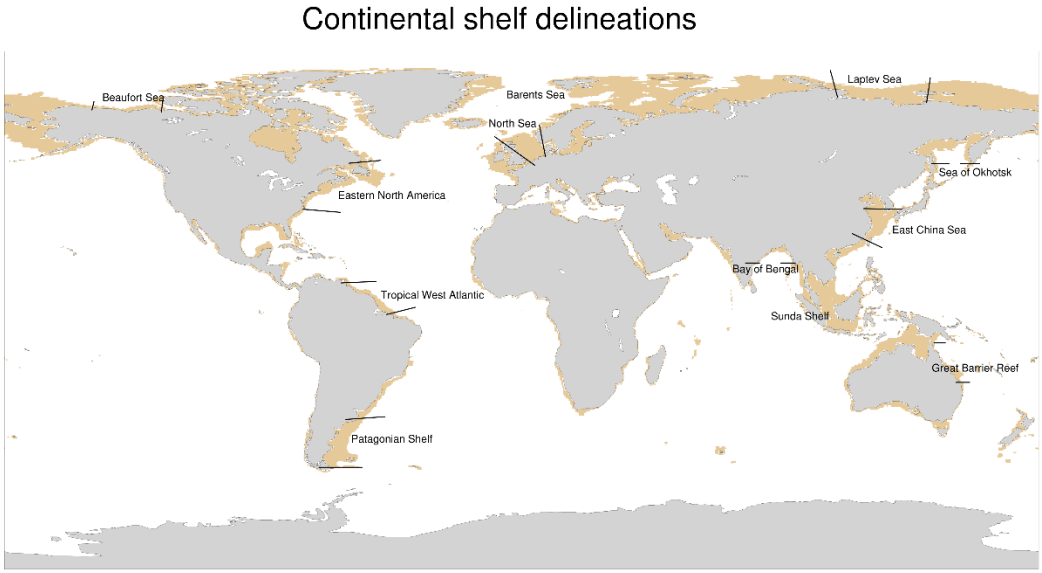

Figure S1. Continental shelf delineation**s.**

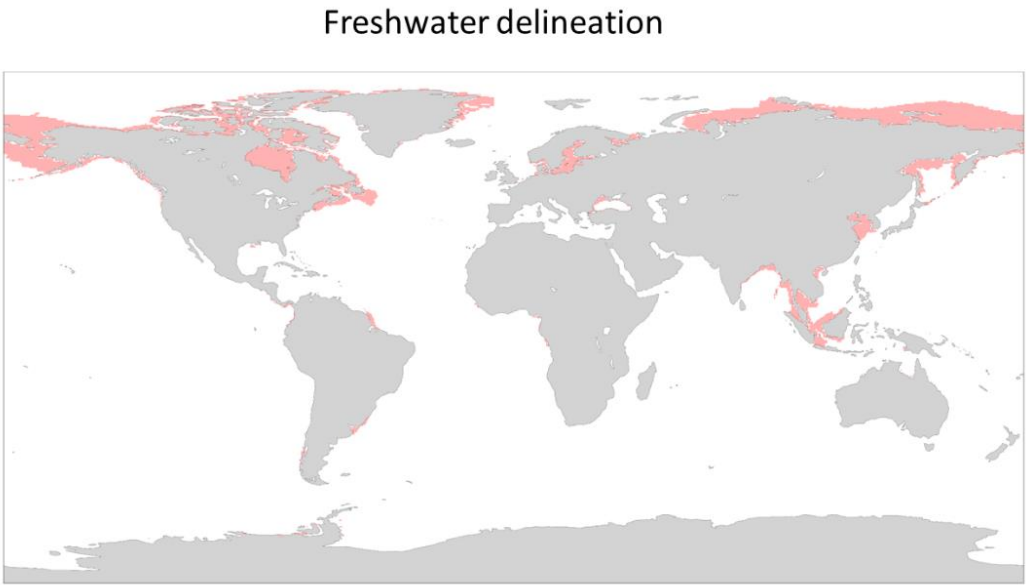

Figure S2. Continental shelf delineation of shelf regions where the surface salinity deviates by more than one standard deviation of the mean oceanic surface salinity.

Text S2. Riverine Loads

- **DIC/Alk**

Catchment yields of DIC and Alk were derived from driving the spatial weathering release model of Hartmann et al. (2009), modified as described in described in Goll et al. (2014), with pre-industrial runoff and temperature data from the Max Planck Institute Earth System Model (MPI-ESM CMIP5, Giorgetta et al. (2013)). As described Lacroix et al. (2019), the yields were calculated as a function of runoff, temperature, lithology and soil properties. Weathering of silicate and carbonate lithologies reactions produce HCO3- ions, thus DIC to Ac in a ratio of 1:1. The alkalinity is assumed to be transported by rivers passively (Ludwig et al., 1998). We neglect the DIC source from soil dissolved CO2, which we assumed to be returned to the atmosphere to a large degree during its transport in rivers. Therefore, we also assumed an Ac to DIC ratio of 1:1 at river mouths, which reflects field observations in the vast majority of rivers (e.g., in Araujo et al. (2014) for tropical Atlantic catchments). In catchments highly affected by organic soil exports, the DIC might deviate from the HCO_3^- concentrations, but rarely by more than 10 % (Meybeck and Vörösmarty, 1999). We performed modifications with respect to Lacroix et al. (2019) based off comparisons with observations (Tank et al., 2012) for major Arctic catchments. The global DIC load of 0.37 Pg yr^{-1} provided by the approach is within the estimate range of 0.26-0.55 Pg yr^{-1} (Lacroix et al. (2020) and citations therein).

- **Terrestrial organic matter**

We derived tDOM catchment exports from the DOC exports provided by the Global Nutrient Export from WaterSheds 2 (NEWS2) study (Mayorga et al., 2010; Seitzinger et al., 2010). The NEWS2 terrestrial model performs multiple regressions with environmental drivers to calculate nutrients and carbon export from watersheds at a 0.5 degree resolution (Harrison et al., 2005). The tDOM exports were thereby scaled to represent the more recently acknowledged estimate of around 0.24 Tg C yr^{-1} (Hedges et al., 1997; Cai, 2011; Bauer et al., 2013; Aarnos et al., 2018), which represented a significant increase with respect to the range simulated by the NEWS model (0.14-0.17 Pg C yr^{-1}) used in Lacroix et al. (2019). The tDOM C:P weight ratio of 1000 was derived from Meybeck (1982), where global measurements of DOP and DOC were extrapolated globally and confirmed in Compton et al. (2000). In the model study NEWS2, a natural C:P weight ratio of 425 for tDOM is suggested. We also assumed a tDOM N:P mole ratio of 16:1 out of simplicity, although we found very close estimates to this in literature for global loads (Meybeck, 1982; Seitzinger et al., 2005, 2010).

The exports of riverine POM were derived from the POC exports of the Beusen et al. (2005) model output generated by NEWS2 (Seitzinger et al., 2010). We added riverine POM to the oceanic POM pool, with the reasoning that riverine POM C:N:P ratios found in literature are closer to oceanic POM than for tDOM. The POM mole C:P ratio thereby was reported to range from 57:1 to 315:1 according to Meybeck (1982) and Ramirez and Rose (1992). The global POM C:N:P:Fe ratio were chosen to be 122:16:1:3.0 10-4. The processing of POM in the coastal ocean is also suggested to be relatively efficient, although this depends on the POM composition, as well shelf characteristics (Blair and Aller, 2011).

- **Phosphorus**

The phosphorus inputs to river catchments were assumed to consist of weathering and non-weathering exports to the catchments. The weathering release was calculated as in the study of Hartmann et al. (2014), where the yields are also described as a function of runoff, temperature, lithology and soil properties, with the runoff and temperature extracted from the MPI-ESM CMIP5 pre-industrial output. The non-weathering sources of phosphorus included fertilizer (Hart et al., 2004), sewage (Morée et al., 2013) and allochthonous (Beusen et al., 2016) input estimations for the year 1900, as done in (Beusen et al., 2016). These non-weathering inputs were distributed globally according to the spatial distribution of present day anthropogenic DIP exports (NEWS2). Part of the P inputs to the catchments was assumed to be transformed to organic matter during its residence on land and in rivers. To determine how much of the riverine P load was contained within organic matter and eliminated from the inorganic catchment pool, we used the stoichiometry of the organic matter (P:C = 1:122 for riverine POM and P:C = 1:2583 for tDOM). The remaining P was assumed to be inorganic P:

$$\mathbf{(1)}\quad IP_{catch} = P_{total,catch} - P_{tDOM,catch} - P_{POM,catch}$$

with IPcatch being the inorganic catchment load of inorganic phosphorus, Ptotal,catch the sum of weathering and non-weathering catchment inputs, PPOM,catch the fraction of catchment inputs of P transformed into POM and PDOM,catch the fraction of catchment inputs of P transformed into tDOM.

- **Silica, Iron**

The DSi export to the ocean was obtained by driving the Beusen et al. (2009) model with MPI-ESM CMIP5 precipitation output. The global load of 168 Tg Si yr^{-1} is comparable to recent estimates of 158 – 200 Tg SiO_2 yr^{-1} (Lacroix et al., 2019). We did not consider the biological availability of particulate silica, although this might be considerable (Tréguer and De La Rocha, 2013).

DIN and DFe riverine loads were quantified by using fixed ratios of DIP:DIN = 1:16 and DIP:DFe = 1:3.0 10^{-4}. Both N and Fe were also contained in organic matter at the same ratios in relation to phosphorus. The calculated global export of N of 27 Tg N yr^{-1} is between the purely natural flux estimate of 21 Tg N yr^{-1} (Green et al., 2004) and 1970 exports of 38 Tg N yr^{-1} (NEWS2).

Text S3. Organic matter degradation sensitivity simulations

- **Coastal sediment organic matter**

The pre-industrial state of the ocean was achieved by forcing the LR (1.5 degrees spatial resolution) ocean model with OMIP forcing and using a constant atmospheric CO_2 concentration of 278 ppm (Etheridge et al., 1996). We first performed simulations to test different sediment POM remineralization rates (0.0013 d^{-1}, 0.0026 d^{-1}, 0.0069 d^{-1}) for 200 years.

The altered continental shelf sediment POM remineralization rates of 0.0026 d^{-1} and 0.0068 d^{-1} produce a substantial increase of the continental shelves NPP in the model as a result of the enhanced recycling of nutrients and their subsequent mixing back into the shallow water column, while at the 0.0013 d^{-1} rate the NPP we do not observe a substantial change to the standard deep ocean rate of 0.001 d^{-1} that is used in the standard model. The global distributions for the open ocean of the NPP remain almost identical however (i.e. for the 0.0026 d^{-1} rate shown in Figure S1).

The simulations produce POM shelf deposition to shelf burial efficiency rates of 67 %, 15 % and 7 % and shelf POM contributions to the global burial of 80 %, 74 % and 49 % for POM remineralization rates of 0.0013 d^{-1}, 0.0026 d^{-1} and 0.0068 d^{-1} respectively. The burial of POM on the shelves is thus almost null when using a remineralization rate of 0.0068 d^{-1} and was not significant at the global scale, contradicting substantial shelf burial rates of POM reported in literature. On the other hand, the 0.0013 d^{-1} rate recycled only a small part of the POM deposited in the sediment. In reviews of literature estimates, Krumins et al. (2013) report a shelf burial to shelf deposition range of 8-23 %, and Chen and Borges (2009) report a burial contribution to the global burial of around 50-80 % for POM. The agreement organic matter burial rates on the global shelf is therefore best reflected at the rate of 0.0026 d^{-1}, retained the 0.0026 d^{-1} for the main manuscript simulations as well as further LR simulations presented in the Supplementary Information.

Despite similar open ocean NPP distributions, we observe an increase in the shelf NPP contribution, with the most pronounced increases in the East China Sea, the North Sea, on the tropic West Atlantic shelf, the eastern North American shelf and the Louisiana Shelf at the rate of 0.0026 d^{-1} (Figure S1). At the standard model remineralization rate of 0.001 d^{-1}, these regions show very low biological productivity. A high NPP on shallow continental shelves has been reported by Muller-Karger et al. (2005) an analysis of a satellite-based NPP data-product, as well as in the Sea-viewing Wide Field-of-view Sensor (SeaWiFS) data-product.

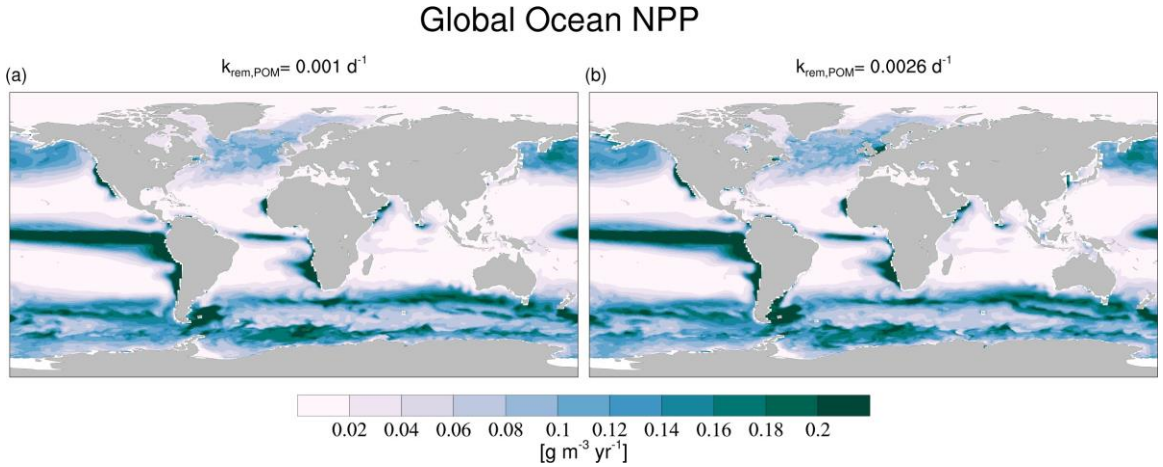

Figure S3. Continental shelf delineation**s.**

- tDOM

Because of the large uncertainties associated with the breakdown of tDOM in the ocean, we performed simulations to test a range of tDOM degradation rates in the ocean:

$T_{tDOM,inst}$ = 0 years
$T_{tDOM,labile}$ = 0.3 year
$T_{tDOM,photoox}$ = light-dependent
$T_{tDOM,semi\text{-}labile}$ = 1.5 years
$T_{tDOM,semi\text{-}ref}$ = 20 years

We performed LR simulations over 2'000 years for the 5 tDOM mineralization scenarios ($T_{tDOM,labile}$, $T_{tDOM,labile}$, $T_{DOM,photoox}$, $T_{DOM,semi\text{-}labile}$, $T_{DOM,semi\text{-}ref}$), starting from a spin-up of the sediment module of 5'000 years for the new shelf sediment POM remineralization rate. These simulations accounted for two different types of tDOM degradation pathways in the ocean. The first pathway ($T_{tDOM,labile}$, $T_{tDOM,labile}$, $T_{DOM,semi\text{-}labile}$, $T_{DOM,semi\text{-}ref}$) assumes that that the degradation of tDOM is solely a function of tDOM and oxygen concentrations (therefore representing purely biotic breakdown). The lifetimes were chosen to represent the tDOM lifetime in the case of instantaneous mineralization at the river mouth, e.g., assumed in Bernard et al. (2011) and Bourgeois et al. (2016), the lifetime of labile tDOM mineralization suggested in Fichot and Benner (2014), as well as the lifetimes of semi-labile and semi-refractory oceanic DOM suggested in Hansell et al. (2012). We did not consider a fully refractory rate (Hansell et al., 2012), due to its lifetime of over 20'000 years exceeding sensible model simulation lengths, and the lack of observation of considerable amounts of tDOM in the open ocean. The second pathway ($T_{tDOM,photoox}$) represents the photodegradation breakdown effect that is caused by the exposure of abiotic tCDOM to shortwave radiation.

Under the first breakdown pathway, tDOM is mineralized as a function of the tDOM concentrations and a oxygen limitation function ΓO_2, which only allows degradation when oxygen concentrations are higher than the threshold concentration (thresaerob=5 10-2 µ M O2):

$$\frac{dtDOM}{dt} = k_{rem,tDOM} * tDOM * \Gamma_{O_2} \qquad (2)$$

With krem,tDOM being the mineralization rate (d^{-1}) and tDOM the tDOM concentration (kmol C m^{-3}). The krem,tDOM rates were derived solving the Eq. 2 with (TtDOM,labile, TtDOM,labile, TDOM,semi-labile and TDOM,semi-ref). The approximation given by the equation is only valid if oxygen limitation does not play a large major role in the limitation of the tDOM degradation (Eq. 3.4).

The second breakdown pathway included the breakdown of biologically unreactive chromophoric dissolved organic material (tCDOM). We assumed that 20 % of the tDOM

loads consisted of biologically reactive tDOM that was mineralized according to Equation 2 with $T_{tDOM,labile}$, whereas 80 % of the tDOM consisted of biologically unreactive tCDOM, which was partly photooxidized. To derive the photooxidation parametrization, we used the averaged tDOM breakdown rates measured on the Louisiana Shelf given in Fichot and Benner (2014) for all 4 seasons, and fitted a linear relationship between these values and the averaged modelled regional surface shortwave radiation in these regions. We also set a minimum rate of degradation, corresponding to a tCDOM lifetime of 20 years (semi-refractory rate as described in Hansell et al. (2012)). The breakdown process was suggested to be due to combined biotic and abiotic breakdown, as suggested in Fichot and Benner (2014):

$$\frac{dtDOM}{dt} = \frac{dk_{rem,shwav}}{dr_{shwav}} * tCDOM * \Gamma_{O_2} \quad (4)$$

with $k_{rem,shwav}$ being the averaged regional tCDOM breakdown rates in the Fichot and Benner (2014) study and r_{shwav}. the averaged regional surface shortwave radiation in the model for the given seasons. The oxygen threshold used was also $thres_{aerob}$=5 10^{-2} µ M O_2.

The validation of the tDOM breakdown rate via photodegradation was done by comparing the contribution of tDOM to the total oceanic DOM for different open ocean basins (Opsahl and Benner, 1997; Hernes and Benner, 2002; Benner et al., 2005), regional tDOM budget studies (Fichot and Benner, 2014; Kaiser et al., 2017), as well as in a comparison with regional tCDOM photodegradation rates measured in Aarnos et al. (2018) for the photodegradation pathway. The quantification of the shortwave radiation in the water column, which depends on the radiation, the light spectrum and the absorption by water and phytoplankton, is described in Paulsen et al. (2018).

tDOM reactivity scenarios	*tDOM river loads*	$k_{rem,tDOM}$	*Theoretical tDOM residence time* $k_{rem,tDOM-1}$	*Global oceanic tDOM inventory*	*Model residence time*	*Average modelled surface removal rate*
	[Tg C yr^{-1}*]*	*[*d^{-1}*]*	*[d]*	*[Tg C]*	*d*	*[Mg C* d^{-1}*]*
(a) $T_{tDOM,inst}$	230	-	-	-	-	-
(b) $T_{tDOM,labile}$	230	0.008	125	95.6	131	2.9
(c) $T_{tDOM,photoox}$	230(180)	-	-	461(262)	731(145)	3.4(3.2)
(d) $T_{tDOM,semi-labile}$	230	0.002	547	333	529	1.3
(e) $T_{tDOM,semi-ref}$	230	0.0001	7300	>1487*	>2349*	0.4*

Table S1. tDOM inventories and removal rates. The lighter values in the (c) row represent the values for the photooxidation of tCDOM. A steady state for tDOM in (e) was not reached.

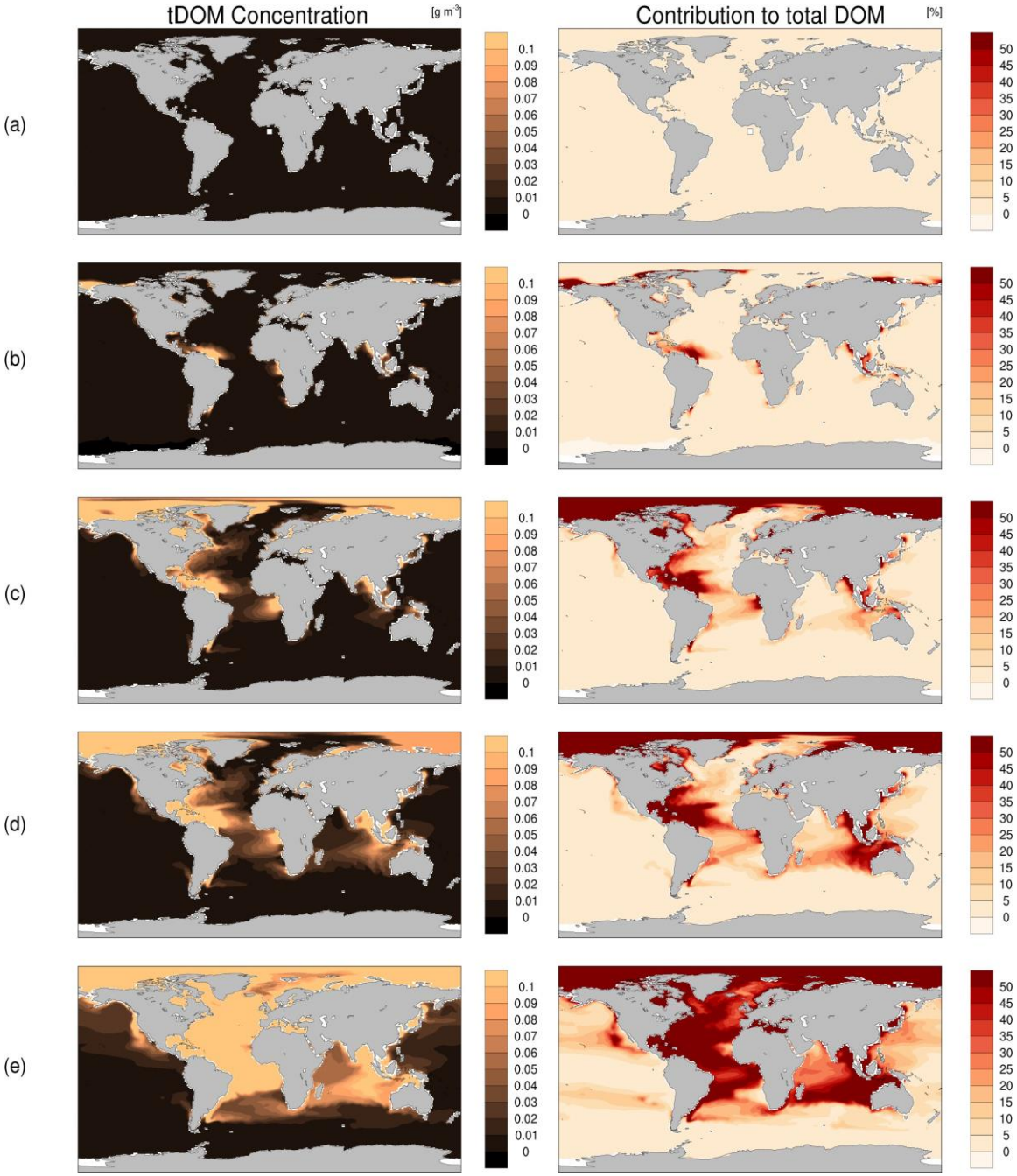

Figure S4. Left panels are the tDOM surface concentrations (reported in g C m^{-3} yr^{-1}) and right panels are the fractions of tDOM to total surface layer DOM concentrations [%] for (a) TtDOM,inst, (b) TtDOM,labile, (c) TtDOM,photoox, (d) TtDOM,semi-labile and (e) TtDOM,semi-ref tDOM degradation scenarios.

	tDOM degradation			
	Observed		Modelled	
Louisiana Shelf				
Annual mean	0.68 (44%)	1.75 (35%)	1.22 (25%)	0.39 (8%)
Summer	0.341	0.55	0,47	0,04
Winter	0.07	0.51	0,21	0,03
Baltic (Year mean)	1.75 (40%)	2.32 (82%)	2.29 (81%)	2.09 (74%)
Arctic (Year mean)	12.2 (54%)	16.9 (69%)	9.5 (39%)	1.29 (5%)
		$T_{tDOM,labile}$	$T_{tDOM,photoox}$	$T_{tDOM,semi\text{-}labile}$

Table S2. tDOM inventories and removal rates. The lighter values in the (c) row represent the values for the photooxidation of tCDOM. A steady state for tDOM in (e) was not reached.

River	*Observed tDOM photo-mineralization* [Tg C yr^{-1}]	*Modelled tDOM photo-mineralization* [Tg C yr^{-1}]
Amazon	6.98	5.58
Congo	3.04	1.43
Danube	0.08	0.36
Ganges-Brahmaputra	0.13	0.32
Lena	1.36	0.44
Mekong	0.13	0.04
Mississippi	0.24	0.74
Parana	0.23	0.11
St Lawrence	0.07	0.43
Yangtze	0.23	0.28

Table S3. Comparison of modelled photo-mineralization rates with rates measured in plumes from Aarnos et al. (2018).

S.5 Modelled main simulation nutrient concentration

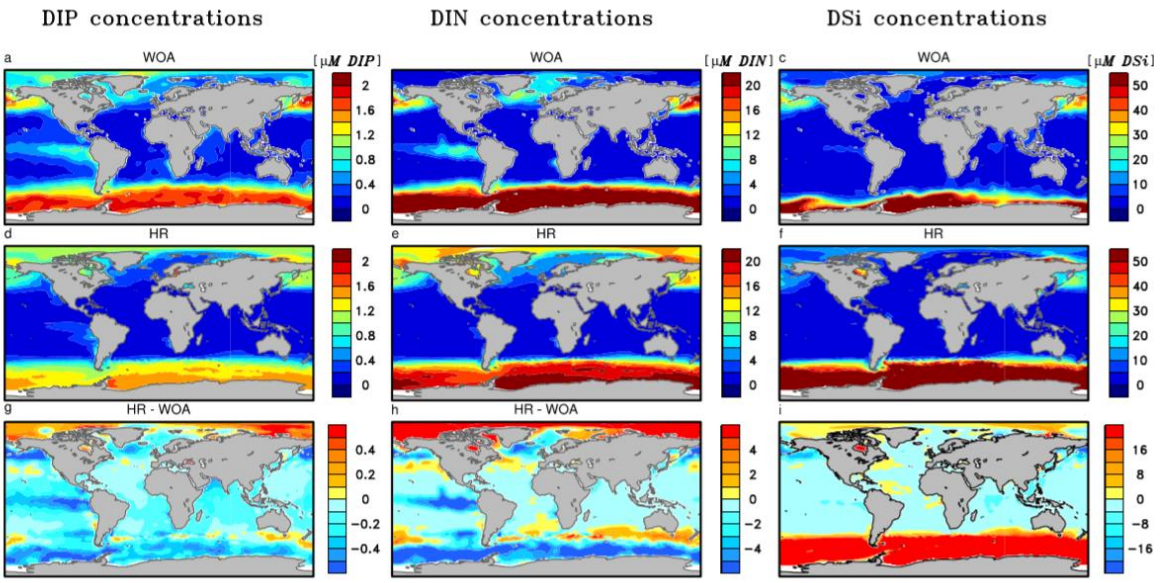

Figure 6. Surface DIP (a,d,g), DIN (b,e,h) and DSi (c,f,i) concentrations from WOA observations (a,b,c), the main HR simulation used in this manuscript (d,e,f) and their differences HR-WOA (g,h,i).

S.6. Residence time k_{exp} values

Regions/*Plumes*	k_{exp} **[mths^{-1}]**	$K_{exp,95\%min}$ **[mths^{-1}]**	$K_{exp,95\%max}$ **[mths^{-1}]**
All shelf waters	*0.07*	*0.08*	*0.06*
Shelf surface waters	*0.07*	*0.08*	*0.06*
Freshwater	*0.29*	*0.33*	*0.26*
Laptev Sea	0.01	0.01	0.01
Beaufort Sea	0.01	0.15	0.14
Sea of Okhotsk	0.06	0.07	0.06
North Sea	0.08	0.09	0.07
South Atlantic Bight	0.81	0.94	0.68
East China Sea	0.07	0.08	0.07
Bay of Bengal	0.49	0.54	0.45
Sunda Shelf	0.21	0.25	0.18
Tropical West Atlantic	1.83	1.88	1.77
Great Barrier Reef	0.41	0.43	0.40
Patagonia	0.04	0.05	0.04
Amazon Plume	*1.85*	*1.86*	*1.83*
Congo Plume	*0.64*	*0.66*	*0.61*
Ganges Plume	*1.39*	*1.70*	*1.08*

Table S4. k_{exp} values and their 90% confidence intervals for regions shown in Figure 2 of the manuscript.

S.7. FCO_2 comparisons to previous estimates

Regions/*Plumes*	**Modelled FCO_2 [$TgCyr^{-1}$]**	**FCO_2 estimates [$Tg\ Cyr^{-1}$]**
Laptev Sea	1.7	*<-0.01*
Beaufort Sea	*-0.1*	-4
Sea of Okhotsk	-2.1	-14
North Sea	-16	-9 to -17
South Atlantic Bight	-0.7	-1 to -5
East China Sea	-4	-19
Bay of Bengal	2.6	-0.5
Sunda Shelf	-1.1	-1.0
Tropical West Atlantic	8	0.4
Great Barrier Reef	-1.0	-1.6
Patagonia	-9	-18

Table 7. Simulated annual mean FCO_2 for the present day in comparison to a compilation of previous regional estimates compiled from Thomas et al. (2004), Chen et al. (2009), Laruelle et al. (2014), Fennel et al. (2019).

References

Aarnos, H., Ylöstalo, P., and Vähätalo, A. V.: Seasonal phototransformation of dissolved organic matter to ammonium, dissolved inorganic carbon, and labile substrates supporting bacterial biomass across the Baltic Sea, Journal of Geophysical Research: Biogeosciences, 117, https://doi.org/10.1029/2010JG001633, 2012.

Aarnos, H., Gélinas, Y., Kasurinen, V., Gu, Y., Puupponen, V.-M., and Vähätalo, A. V.: Photochemical Mineralization of Terrigenous DOC to Dissolved Inorganic Carbon in Ocean, Global Biogeochemical Cycles, 32, 250–266, https://doi.org/10.1002/2017GB005698, 2018.

Araujo, M., Noriega, C., and Lefèvre, N.: Nutrients and carbon fluxes in the estuaries of major rivers flowing into the tropical Atlantic, Frontiers in Marine Science, 1, 1–16, https://doi.org/10.3389/fmars.2014.00010, 2014.

Bauer, J. E., Cai, W.-J., Raymond, P. A., Bianchi, T. S., Hopkinson, C. S., and Regnier, P. A. G.: The changing carbon cycle of the coastal ocean, Nature, 504, 61, 2013.

Bélanger, S., Cizmeli, S. A., Ehn, J., Matsuoka, A., Doxaran, D., Hooker, S., and Babin, M.: Light absorption and partitioning in Arctic Ocean surface waters: impact of multiyear ice melting, Biogeosciences, 10, 6433–6452, https://doi.org/10.5194/bg-10-6433-2013, https: //www.biogeosciences.net/10/6433/2013/, 2013.

Benner, R., Louchouarn, P., and Amon, R. M. W.: Terrigenous dissolved organic matter in the Arctic Ocean and its transport to surface and deep waters of the North Atlantic, Global Biogeochemical Cycles, 19, https://doi.org/10.1029/2004GB002398, https://doi.org/10.1029/ 2004GB002398, 2005.

Bernard, C. Y., Dürr, H. H., Heinze, C., Segschneider, J., and Maier-Reimer, E.: Contribution of riverine nutrients to the silicon biogeochemistry of the global ocean – a model study, Biogeosciences, 8, 551–564, https://doi.org/10.5194/bg-8-551-2011, 2011.

Beusen, A. H. W., Dekkers, A. L. M., Bouwman, A. F., Ludwig, W., and Harrison, J.: Estimation of global river transport of sediments and associated particulate C, N, and P, Global Biogeochemical Cycles, 19, https://doi.org/10.1029/2005GB002453, 2005.

Beusen, A. H. W., Bouwman, A. F., Dürr, H., Dekkers, A. L. M., and Hartmann, J.: Global patterns of dissolved silica export to the coastal zone: Results from a spatially explicit global model, Global Biogeochemical Cycles, 23, https://doi.org/10.1029/2008GB003281, 2009.

Blair, N. E. and Aller, R. C.: The Fate of Terrestrial Organic Carbon in the Marine Environment, Annual Review of Marine Science, 4, 401–423, https://doi.org/10.1146/annurev-marine-120709-142717, 2011.

Compton, J., Mallinson, D., Glenn, C., Filippelli, G., Föllmi, K., Shields, G., and Zanin, Y.: Variations in the global phosphorus cycle, IN:Marine Authigenesis: From Global to Microbial, Wiley-Blackwell, pp. 21–33, 2000.

Etheridge, D. M., Steele, L. P., Langenfelds, R. L., Francey, R. J., Barnola, J.-M., and Morgan, V. I.: Natural and anthropogenic changes in atmospheric CO2 over the last 1000 years from air in Antarctic ice and firn, Journal of Geophysical Research: Atmospheres, 101, 4115–4128, https://doi.org/10.1029/95JD03410, 1996.

Fichot, C. G. and Benner, R.: The fate of terrigenous dissolved organic carbon in a river-influenced ocean margin, Global Biogeochemical Cycles, 28, 300–318, https://doi.org/10.1002/2013GB004670, 2014.

Gattuso, J.-P., Frankignoulle, M., and Wollast, R.: CARBON AND CARBONATE METABOLISM IN COASTAL AQUATIC ECOSYS-

TEMS, Annual Review of Ecology and Systematics, 29, 405–434, https://doi.org/10.1146/annurev.ecolsys.29.1.405, https://doi.org/10. 1146/annurev.ecolsys.29.1.405, 1998.

Giorgetta, M. A., Jungclaus, J., Reick, C. H., Legutke, S., Bader, J., Böttinger, M., Brovkin, V., Crueger, T., Esch, M., Fieg, K., Glushak, K., Gayler, V., Haak, H., Hollweg, H.-D., Ilyina, T., Kinne, S., Kornblueh, L., Matei, D., Mauritsen, T., Mikolajewicz, U., Mueller, W., Notz, D., Pithan, F., Raddatz, T., Rast, S., Redler, R., Roeckner, E., Schmidt, H., Schnur, R., Segschneider, J., Six, K. D., Stockhause, M., Timmreck, C., Wegner, J., Widmann, H., Wieners, K.-H., Claussen, M., Marotzke, J., and Stevens, B.: Climate and carbon cycle changes from 1850 to 2100 in MPI-ESM simulations for the Coupled Model Intercomparison Project phase 5, Journal of Advances in Modeling Earth Systems, 5, 572–597, https://doi.org/10.1002/jame.20038, 2013.

Green, P. A., Vörösmarty, C. J., Meybeck, M., Galloway, J. N., Peterson, B. J., and Boyer, E. W.: Pre-industrial and contemporary fluxes of nitrogen through rivers: a global assessment based on typology, Biogeochemistry, 68, 71–105, https://doi.org/10.1023/B:BIOG.0000025742.82155.92, 2004.

Hansell, D. A., Carlson, C. A., and Schlitzer, R.: Net removal of major marine dissolved organic carbon fractions in the subsurface ocean, Global Biogeochemical Cycles, 26, https://doi.org/10.1029/2011GB004069, https://www.scopus.com/inward/record.uri?eid=2-s2. 0-84856755461{&}doi=10.1029{%}2F2011GB004069{&}partnerID=40{&}md5=c6204e9edf6e9611da77c548c7127666, 2012.

Harrison, J. A., Caraco, N., and Seitzinger, S. P.: Global patterns and sources of dissolved organic matter export to the coastal zone: Results from a spatially explicit, global model, Global Biogeochemical Cycles, 19, https://doi.org/10.1029/2005GB002480, 2005.

Hartmann, J., Jansen, N., Dürr, H. H., Kempe, S., and Köhler, P.: Global CO2-consumption by chemical weathering: What is the contribution of highly active weathering regions?, Global and Planetary Change, 69, 185–194, https://doi.org/https://doi.org/10.1016/j.gloplacha.2009.07.007, 2009.

Hartmann, J., Moosdorf, N., Lauerwald, R., Hinderer, M., and West, A. J.: Global chemical weathering and associated P-release — The role of lithology, temperature and soil properties, Chemical Geology, 363, 145–163, https://doi.org/https://doi.org/10.1016/j.chemgeo.2013.10.025, http://www.sciencedirect.com/science/article/pii/S0009254113004816, 2014.

Hedges, J. I., Keil, R. G., and Benner, R.: What happens to terrestrial organic matter in the ocean?, Organic Geochemistry, 27, 195–212, https://doi.org/https://doi.org/10.1016/S0146-6380(97)00066-1, 1997.

Hernes, P. J. and Benner, R.: Transport and diagenesis of dissolved and particulate terrigenous organic matter in the North Pacific Ocean, Deep Sea Research Part I: Oceanographic Research Papers, 49, 2119–2132, https://doi.org/https://doi.org/10.1016/S0967-0637(02)001280, http://www.sciencedirect.com/science/article/pii/S0967063702001280, 2002.

Holmes, R. M., McClelland, J. W., Raymond, P. A., Frazer, B. B., Peterson, B. J., and Stieglitz, M.: Lability of DOC transported by Alaskan rivers to the Arctic Ocean, Geophysical Research Letters, 35, https://doi.org/10.1029/2007GL032837, https://doi.org/10.1029/ 2007GL032837, 2008.

Johannessen, S. C., Miller, W., and Cullen, J.: Calculation of UV attenuation and colored dissolved organic matter absorption spectra from measurement of ocean color, vol. 108, https://doi.org/10.1029/2000JC000514, 2003.

Kaiser, K., Canedo-Oropeza, M., McMahon, R., and Amon, R. M. W.: Origins and transformations of dissolved organic matter in large Arctic rivers, Scientific Reports, 7, 13064, https://doi.org/10.1038/s41598-017-12729-1, 2017.

Krumins, V., Gehlen, M., Arndt, S., Van Cappellen, P., and Regnier, P.: Dissolved inorganic carbon and alkalinity fluxes from coastal marine sediments: Model estimates for different shelf environments and sensitivity to global change, Biogeosciences, 10, 371–398, https://doi.org/10.5194/bg-10-371-2013, 2013.

1–56, https://doi.org/10.5194/bg-2019-152, https://www.biogeosciences-discuss.net/bg-2019-152/, 2019.

Lalonde, K., Vähätalo, A. V., and Gélinas, Y.: Revisiting the disappearance of terrestrial dissolved organic matter in the ocean: a δC13 study, Biogeosciences, 11, 3707–3719, https://doi.org/10.5194/bg-11-3707-2014, 2014.

Ludwig, W., Amiotte-Suchet, P., Munhoven, G., and Probst, J.-L.: Atmospheric CO2 consumption by continental erosion: present-day controls and implications for the last glacial maximum, Global and Planetary Change, 16-17, 107–120, https://doi.org/https://doi.org/10.1016/S0921-8181(98)00016-2, http://www.sciencedirect.com/science/article/pii/S0921818198000162, 1998.

Meybeck, M.: Carbon, Nitrogen, and Phosphorus Transport by World Rivers, Am. J. Sci., 282, 1982.

Meybeck, M. and Vörösmarty, C.: Global transfer of carbon by rivers, Global Change News Lett, 26, 1999.

Meybeck, M., Dürr, H. H., and Vörösmarty, C. J.: Global coastal segmentation and its river catchment contributors: A new look at land-ocean linkage, Global Biogeochemical Cycles, 20, https://doi.org/10.1029/2005GB002540, 2006.

Opsahl, S. and Benner, R.: Distribution and cycling of terrigenous dissolved organic matter in the ocean, Nature, 386, 480–482,

https://doi.org/10.1038/386480a0, https://doi.org/10.1038/386480a0, 1997.

Paulsen, H., Ilyina, T., Jungclaus, J. H., Six, K. D., and Stemmler, I.: Light absorption by marine cyanobacteria affects tropical climate mean state and variability, Earth System Dynamics, 9, 1283–1300, https://doi.org/10.5194/esd-9-1283-2018, https://www.earth-syst-dynam.net/ 9/1283/2018/, 2018.

Ramirez, A. J. and Rose, A. W.: Analytical geochemistry of organic phosphorus and its correlation with organic carbon in marine and fluvial sediments and soils, American Journal of Science, 292, 421–454, https://doi.org/10.2475/ajs.292.6.421, 1992.

Seidel, M., Manecki, M., Herlemann, D. P. R., Deutsch, B., Schulz-Bull, D., Jürgens, K., and Dittmar, T.: Composition and Transformation of Dissolved Organic Matter in the Baltic Sea, Frontiers in Earth Science, 5, 1–20, https://doi.org/10.3389/feart.2017.00031, 2017.

Søndergaard, M. and Middelboe, M.: A cross-system analysis of labile dissolved organic carbon, Marine Ecology Progress Series, 118, 283–294, http://www.jstor.org/stable/24849785, 1995.

Tank, S. E., Raymond, P. A., Striegl, R. G., McClelland, J. W., Holmes, R. M., Fiske, G. J., and Peterson, B. J.: A land-to-ocean perspective on the magnitude, source and implication of DIC flux from major Arctic rivers to the Arctic Ocean, Global Biogeochemical Cycles, 26, https://doi.org/10.1029/2011GB004192, 2012.

.